ATMOSPHERIC RE-ENTRY NDI CONTROL DESIGN FOR THE HOPPER RLV CONCEPT

Andrés Marcos, Luis F. Peñín, Augusto Caramagno
DEIMOS SPACE S.L.
Ronda de Poniente VI, P2-2, 28760 Madrid, Spain,
{ *andres.marcos, luis-felipe.penin, augusto.caramagno* }
@deimos-space.com

Josef Sommer, Wolfgang Belau
ASTRIUM SPACE TRANSPORTATION
Huenefeldstrasse 1-5, 28199, Bremen, Germany
{ *josef.sommer, wolfgang.belau* } *@space.eads.net*

Abstract:
In this paper an NDI control design for the automated atmospheric re-entry of the Hopper reusable-launch vehicle (RLV) concept is presented. The NDI design is characterized by *i*) an inversion step where the trim and flight surfaces deflections are independently calculated and *ii*) by avoiding the standard linearization of the known aerodynamic database. The resulting control design is validated through time simulations using a high-fidelity model of the Hopper RLV in the face of parametric and aerodynamic database uncertainties, sensor noise and realistic atmospheric environment.

Keywords: NDI, atmospheric re-entry, attitude control design

1. INTRODUCTION

Nonlinear Dynamic Inversion (NDI) is a theoretically very simple but powerful technique that has been used quite profusely in the last 15 years in the field of flight control. In Space applications is less prevalent but recently has been explored for atmospheric re-entry vehicles (Ito, D. *et al.*, 2002; Da Costa, R.R. *et al.*, 2003) due to the challenging dynamics for this type of missions and the possibility of confronting them –throughout the complete re-entry corridor– by using NDI.

It is well known that the main disadvantages of this technique are the numerical issues associated with the nonlinear inversion step and the lack of explicit robustness guarantees. Indeed, it can be said that NDI addresses stability and performance (including robustness) through the use of other control synthesis techniques, e.g. PID, LQG, H_∞.

In this paper the NDI approach is used to design an atmospheric re-entry attitude controller for the Hopper RLV concept. The NDI design and the associated Dynamic-Kinematic-Environment(DKE) simulator are developed within the framework of the European Space Agency (ESA) study entitled "Health Management System for Reusable Space Transportation" (HMS) AO/1-4781/05/NL/JA and will serve as the testbed for advanced fault detection & isolation and HMS studies.

The NDI approach used has the following features that distinguishes it from previous re-entry NDI designs:

(1) A four step-approach with a mixed Wind/Body-axes formulation is used. This approach is closer to NDI designs for aircraft (in spacecraft quaternions are typically used) and better from a PID-tuning perspective (it decouples the motion of the three axes and can be motivated better from a flight mechanics perspective).
(2) A moment allocation scheme that automates the transitions for the different flight phases based on dynamic pressure and Mach in order to cover the full re-entry trajectory (dyn. pressure for high speed/altitude and Mach for low speed/altitude).
(3) The "pure" inversion step presents a novel decoupling approach based on *flight* and *trim* surface calculation. This approach can be used due to the Hopper's actuation redundancy.

2. THEORETICAL BACKGROUND

Firstly, the essential ideas behind NDI approaches (Honeywell and Lockheed Martin, 1996; Vu, B.D., 1997) are reviewed for an ideal system (no uncertainty, no disturbances and no faults) in order to provide a theoretical background on this technique.

The NDI synthesis method considers a class of nonlinear systems affine in the control input (without loss of generality since it is always possible to transform a nonlinear input into a new affine input):

$$\begin{aligned} \dot{x} &= f(x) + g(x)u \\ y &= h(x) \end{aligned} \tag{1}$$

Where the state and output mappings, $f(x)$ and $h(x)$ respectively, are smooth nonlinear functions of the states x; and the input injection map $g(x)$ is a diffeomorphism (a smooth function whose inverse exists and is also smooth). For simplicity of presentation only the state-input inversion will be treated here, i.e. $h(x) = x$.

Differentiating the output equation until the input signal appears yields:

$$\dot{y} = \dot{x} = f(x) + g(x)u \tag{2}$$

The required number of successive differentiations indicates the system's relative degree, which in this case is one. Furthermore, since this is a state-input problem there are no zero dynamics –an important consideration for NDI control synthesis, see (Vu, B.D., 1997).

In order to define the NDI control law, a control task is chosen (e.g. tracking, regulation, etc) and its associated mathematical formulation is substituted in Equation 2. For example, choosing an error-minimization control objective $\nu = K(x_c - x)$, where K can be designed using a plethora of techniques (LQG, PID, H_∞, etc), leads to:

$$\dot{y}_{des} = \nu = K(x_c - x) = f(x) + g(x)u \tag{3}$$

Rearranging terms, the NDI control law u_{NDI} is:

$$u_{NDI} = g(x)^{-1}[-f(x) + K(x_c - x)] \tag{4}$$

Substitute this NDI control law in the system's state equation and simplify to get:

$$\begin{aligned} \dot{x} &= f(x) + g(x)\left(g(x)^{-1}[-f(x) + K(x_c - x)]\right) \\ &= K(x_c - x) \end{aligned} \tag{5}$$

Which assuming zero command for regulation, $y_c = x_c = 0$, yields the following linear closed loop:

$$\dot{y} = \dot{x} = -Kx = -Ky \;\Rightarrow\; \dot{y} + Ky = 0 \tag{6}$$

A graphical representation of a standard NDI controller architecture is given in Figure 1 where G_u represents the nominal system.

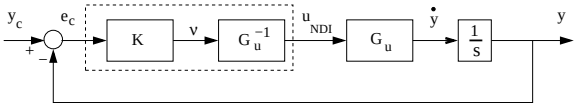

Fig. 1. Standard NDI controller structure.

3. HOPPER RLV AND MISSION PROFILE

The Hopper is a horizontally launch & landing rocket-propelled vehicle comprising a reusable primary stage, the RLV Hopper and one expendable upper stage. It evolved from the FESTIP study and was further elaborated in the scope of the ASTRA program (funded by the German National Agency).

The Hopper executes sub-orbital point-to-point flights of short duration. A typical profile mission comprises acceleration to prescribed sub-orbital staging conditions, cargo ejection, drift to 150 km altitude, automated re-entry, and gliding to one of its dedicated landing sites some 4500 km downrange launch-site, depending on mission inclination. From there the Hopper is transported back to the launch site, where it is prepared for re-flight, see Figure 2. The mission time is less than half an hour and thanks to this, the onboard energy demand is low and the TPS experiences only a quarter of the integral heat load seen by similar re-entries from stable orbits. However, the steepness of the sub-orbital entry drives the maximum of the aerodynamic heating rates and the surface temperatures (1200 degrees Celsius for wing leading edge) to levels comparable with other orbiters.

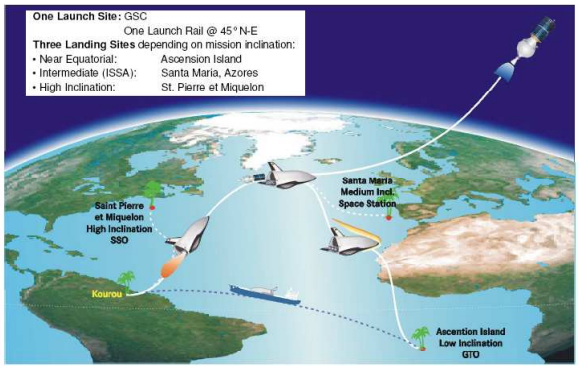

Fig. 2. Hopper Mission Profile.

The aerodynamic configuration features a compact body with rounded edge-like cross section equipped with a delta wing far rear and a central vertical tail. The tapered delta wing has 60^o leading edge sweep, slightly swept back hinge lines of elevons, and slightly sweptback trailing edge. Requirements of a safe landing dictate the wing size, whereas ascent loads govern the dimensioning of the load carrying wing structure.

The aerodynamic controls comprise rudders on the vertical tail capable of $\pm\ 30^o$ symmetric deflection range, inboard and outboard elevons on the wings with symmetric deflection range of $\pm\ 20^o$ and $\pm\ 25^o$ respectively, a fairly large body flap (range of $[-15^o \quad +25^o]$) underneath the main engines, and speed brakes $[0^o \quad +85^o]$ left and right on the engine bay. The inboard and outboard elevons combine the left and right surfaces to form eleron and aileron deflections, furthermore, the inboard surfaces are used predominantly for trim while the outboard for flying.

A RCS is needed to orient and stabilise the vehicle during stage separation, to counteract MECO injection dispersions, and to bring the vehicle into the attitude required for entry. Similar to the American Space Shuttle it is also needed in the high-speed / high

angle-of-attack flight regime to assure control authority down to the transition phase where aerodynamic controls become effective. The RCS is composed of four clusters (each with 3-thrusters) located in the left and right side of the vehicle's front and rear.

The Hopper high-fidelity aerodynamic database was provided by ASTRIUM-ST and consists of nonlinear look-up tables (LUT) dependent on angle of attack, Mach number, sideslip, altitude and the control effectors. Each LUT provides an estimate of the principal stability derivatives and they can be grouped into non-effector and effector-dependent contributors of the aerodynamic coefficients. Furthermore, the database is divided into hypersonic and supersonic/sub-sonic datasets bridged together during a transition phase scheduled on Mach number.

4. RE-ENTRY NDI CONTROL DESIGN

This section presents the nonlinear dynamic inversion (NDI) controller design approach, which provides the necessary effector deflections (RCS and aerosurfaces δ's) based on reference aerodynamic angles (angle of attack α_{ref}, sideslip angle β_{ref} and bank angle σ_{ref}).

The control objectives are established and divided into two categories: level 1 (desirable) and level 2 (required). They consist mainly in robust and accurate tracking of the reference angles and avoidance of control effector saturation. Additionally, robustness objectives pertaining parametric and aerodynamic uncertainties are also given, see Table 1.

Table 1. Control Design Objectives

Tracking error	Level 1: Less than $\pm$ 2 degrees Level 2: Up to +/- 5 degrees for less than 3sec
Angle of attack	Perturbations eliminated within 5-10 sec Limited to 18deg $< \alpha <$ 38deg for M > 10
Bank rate & accel.	Bank rate shall be higher than 15deg/s Bank acceleration higher than $5deg/s^2$
Control effectors	Level 1: Avoid saturation Level 2: Allow saturation for less than 3sec (if not de-stabilizing)
Robustness	Shall be robust to: * Sensor noise * Aerodynamic mismatch * Parametric uncertainty: —- Mass 5 percent —- Ixx, Iyy, Izz 5 percent —- x,z-MRP 0.5 percent —- y-MRP 0.1 percent
Stability	In all cases

The main elements of the Re-entry NDI controller are a PID-plus-rotational-EoM-inversion part, a moment-allocation component and the (aerodynamic) moments-inversion block.

4.1 PID-plus-Rotational-EoM-Inversion component

This component provides the ideal moments required to fulfil the control performance and stability objectives using as inputs the reference aerodynamic angles and a set of measurements.

In order to generate the desired moments from the aerodynamic angles it is necessary to invert the rotational equations of motion in a sequential manner using the following proposed four-step approach. We will describe the sequential process in a reverse order, starting from the calculation of the ideal moments and ending in the use of the reference angles' errors:

The **first step** calculates the ideal moments based on the measured rotational rates p_m, q_m, r_m, a known constant moment of inertia matrix $I_{inertial}$ and desired rotational accelerations $\dot{p}_{des}$, $\dot{q}_{des}$, $\dot{r}_{des}$:

$$\begin{bmatrix} Mx_{ideal} \\ My_{ideal} \\ Mz_{ideal} \end{bmatrix} = I_{inertial} \begin{bmatrix} \dot{p}_{des} \\ \dot{q}_{des} \\ \dot{r}_{des} \end{bmatrix} + \begin{bmatrix} p_m \\ q_m \\ r_m \end{bmatrix} \times \left(I_{inertial} \begin{bmatrix} p_m \\ q_m \\ r_m \end{bmatrix} \right) \tag{7}$$

The **second step** is to find the desired rotational accelerations $\dot{p}_{des}$, $\dot{q}_{des}$, $\dot{r}_{des}$ using the calculated reference rates p_{ref}, q_{ref}, r_{ref}, the measured rates p_m, q_m, r_m and the designed proportional-integral-derivative (PID) control (actually only PI was used at the end):

$$\begin{aligned} \begin{bmatrix} \dot{p}_{des} \\ \dot{q}_{des} \\ \dot{r}_{des} \end{bmatrix} &= \omega_{BW} \begin{bmatrix} p_{error} \\ q_{error} \\ r_{error} \end{bmatrix} = \\ &= \left(P_{pqr} + \frac{I_{pqr}}{s} \right) \left(\begin{bmatrix} p_{ref} \\ q_{ref} \\ r_{ref} \end{bmatrix} - \begin{bmatrix} p_m \\ q_m \\ r_m \end{bmatrix} \right) \end{aligned} \tag{8}$$

Next, the **third step** is to obtain the reference rotational rates p_{ref}, q_{ref}, r_{ref}. We can use the algebraic relationship relating the relative rotation of the wind and body axes with the aerodynamic angles (Durham, W.C., 2001), which can be inverted as follows:

$$\begin{bmatrix} p_{ref} \\ q_{ref} \\ r_{ref} \end{bmatrix} = \Gamma^{-1} \left(\begin{bmatrix} \dot{\alpha}_{des} \\ \dot{\beta}_{des} \\ \dot{\sigma}_{des} \end{bmatrix} - \begin{bmatrix} -q_w \sec\beta \\ r_w \\ \dot{\alpha}_{des} \sin\beta \end{bmatrix} \right) \tag{9}$$

$$\Gamma = \begin{bmatrix} -\cos\alpha\tan\beta & 1 & -\sin\alpha\tan\beta \\ \sin\alpha & 0 & -\cos\alpha \\ -\cos\alpha\cos\beta & -1 & -\sin\alpha\cos\beta \end{bmatrix} \tag{10}$$

This inversion of the kinematic rotational angles facilitates the control design task of tracking reference aerodynamic angles, which is one of the control objectives. Furthermore, this formulation is better for control design and analysis (as it is shown by re-arranging the above two equations using the measurable wind-axes equations):

$$p_{ref} = p_w \cos\alpha - r_w \sin\alpha + \dot{\beta}_{des} \sin\alpha \tag{11}$$

$$q_{ref} = q_w + \dot{\alpha}_{des} \tag{12}$$

$$r_{ref} = p_w \sin\alpha + r_w \cos\alpha - \dot{\beta}_{des} \cos\alpha \tag{13}$$

The above three equations show that it is possible to control, in a decoupled manner, the longitudinal (q_w) and lateral motions (p_w and r_w) using the desired aerodynamic angle rates ($\dot{\alpha}_{des}$ and $\dot{\beta}_{des}$, $\dot{\sigma}_{des}$ respectively).

In the **last step** the desired angle rates are obtained in similar form to Equation 8:

$$\begin{bmatrix} \dot{\alpha}_{des} \\ \dot{\beta}_{des} \\ \dot{\sigma}_{des} \end{bmatrix} = \omega_{BW} \left(\begin{bmatrix} \alpha_{ref} \\ \beta_{ref} \\ \sigma_{ref} \end{bmatrix} - \begin{bmatrix} \alpha_m \\ \beta_m \\ \sigma_m \end{bmatrix} \right) \tag{14}$$

Remark: Due to the good decoupled nature obtained using this four-step approach it is possible to assume during the PID design a longitudinal and lateral/directional decoupling motion. Thus, it is relatively easy to tune the PID gains first for the longitudinal motion and subsequently for the lateral/directional

motion combining both at the end to fine-tune the final PID design.

4.2 Moment-Allocation Component

This component distributes the ideal moments, obtained in the previous component, to the RCS and/or the aerodynamic surfaces.

Three different phases are defined for the moment allocation (resulting in 3 different sets of PID gains in the NDI-plus-Rotational-EoM-Inversion component):

(1) **RCS control phase**: this phase corresponds to the upper part of the re-entry trajectory where there is not enough aerodynamic pressure to use aerodynamic surfaces, and thus the desired moments have to be generated by the RCS.
(2) **Bridging phase**: in this phase, RCS and aerosurfaces are combined to provide the required torque. The atmosphere is not dense enough for the aerosurfaces to have enough control authority alone. This bridging phase is decomposed into three sub-phases each with a different moment allocation scheme.
(3) **Aerodynamic control phase**: this phase correspond to the lower part of the trajectory where the atmosphere is dense permitting the aerodynamic actuators to have enough control authority. There is no need to employ the RCS.

A decision logic block automates the process. It uses the dynamic pressure *qdyn* and Mach number *M* to establish the adequate phase. The first is used for the high speed/altitude phases (RCS and part of Bridging phases) while *M* is used in the remaining phases.

4.3 Aerodynamic-Moment-Inversion component

This is the most well-known and standard component in NDI control technology. Its purpose is to use the ideal aerodynamic coefficients and transform them into the proper control aero-surface deflections that will reproduce these ideal moments for the Hopper.

The ideal coefficients Cl_{id}, Cm_{id}, Cn_{id} are obtained from the allocated ideal aerodynamic moments Mx_{aer}, My_{aer}, Mz_{aer} corrected by the measured BRF-forces (mass m times the measured body accelerations ax, ay, az) and nondimensionalized by the estimated dynamic pressure $qdyn$, the reference surface S and the reference span b and length c:

$$\begin{bmatrix} Cl_{id} \\ Cm_{id} \\ Cn_{id} \end{bmatrix} = \left(\begin{bmatrix} Mx_{aer} \\ My_{aer} \\ Mz_{aer} \end{bmatrix} - r_A \times \begin{bmatrix} ma_x \\ ma_y \\ ma_z \end{bmatrix} \right) / \Omega \qquad \Omega = qdyn \cdot S \cdot \begin{bmatrix} b \\ c \\ b \end{bmatrix} \tag{15}$$

There are two main blocks for this component, the NDI-Coefficient-Calculation and the Aerodynamic-Inversion block:

The **NDI-Coefficient-Calculation block** performs the estimation of the aerodynamic coefficients based on the measured angle of attack α, sideslip β, Mach number and altitude *he*. The approximated aerodynamic database contained in this block is not linearized to any particular trajectory. This has the advantage of resulting in a NDI controller that will accept quite different reference trajectories with minor or none at all updating.

It is highlighted that the stability derivatives have been split into *FLIGHT* and *TRIM* stability derivatives depending on the aerodynamic control effectors they require. This split in the calculations is possible due to the redundancy of the Hopper control effectors.

The **Aerodynamic-Inversion block** performs the inversion of the estimated aerodynamic coefficients Clm_{calc} to obtain the aerodynamic-control deflections required to achieve the desired coefficients $Clmn_{id}$ obtained in Equation 15:

$$\begin{aligned} &Clmn_{id} = CClmn_{calc}(\alpha, M) \cdot H(\delta_1 \dots \delta_n) \\ &\Rightarrow H(\delta_1 \dots \delta_n) = CClmn_{calc}(\alpha, M)^{-1} Clmn_{id} \end{aligned} \tag{16}$$

The matrix $H(\ \delta\ 1\ \dots\ \delta\ n)$ represents the polynomial dependence of the stability derivatives $CClmn_{calc}$ on the deflection surfaces. This dependence is not linear and thus an approach is needed to extract the individual deflections, which is accomplished by linearizing the current effector injection matrix $H(\delta_1 \dots \delta_n)_k$ around the previous deflection values $(\delta_1 \dots \delta_n)_{k-1}$ in order to calculated the new deflection $(\delta_1 \dots \delta_n)_k$:

$$\begin{aligned} &H(\delta_1 \dots \delta_n)|_k \approx H(\delta_1 \dots \delta_n)|_{k-1} \\ &+ \frac{\partial H(\delta_1 \dots \delta_n)}{\partial \delta}|_{k-1} \left(\begin{bmatrix} \delta_1 \\ \vdots \\ \delta_n \end{bmatrix}_k - \begin{bmatrix} \delta_1 \\ \vdots \\ \delta_n \end{bmatrix}_{k-1} \right) \end{aligned} \tag{17}$$

The above inversion and linearization operation are performed for each of the two *trim* and *flight* control effector sets (actually the later contains a subset of the first set). In this manner, the task of the calculated *trim* is to compensate for the equilibrium trajectory (rather than uploading a trim-equilibrium LUT for each possible trajectory) and the inversion of the *flight* set calculates the deflections to track the trajectory (improving robustness).

5. TIME SIMULATIONS

In this section we evaluate the performance of the NDI controller in tracking (but without a guidance component) the ASTRIUM-provided optimal re-entry reference trajectory.

All the time simulations presented were performed using a Dynamic-Kinematic-Environment (DKE) simulator, specifically developed in the course of this study, with the following characteristics:

(1) Full 6 DoF RLV dynamics for atmospheric re-entry (incl. Earth angular velocity effects).
(2) The ASTRIUM-ST high-fidelity Hopper aerodynamic database. Randomly perturbed for each simulation to simulate mismatch with the database used within the NDI control.
(3) Atmospheric environment, the 1962 USSA atmospheric model, and ellipsoidal planet shape.
(4) Actuator (aerodynamic and RCS) models with magnitude and rate saturations.
(5) Sensor models with noise corruption.

A Monte-Carlo campaign is performed, randomly varying the uncertainty present in the system. The uncertainty is modelled using the well-known multiplicative model (Zhou, K. *et al.*, 1996), which allows defining the uncertainty in terms of percentage variations with respect to nominal values. The nature of the uncertainty considered in the Hopper RLV comes from two different sources, parametric uncertainty and aerodynamic mismatch.

The parametric uncertainty arises due to the imperfect knowledge we have for some critical parameters. For example, the mass of the vehicle is perfectly known during the simulation but it is not so well estimated during a real flight due to changes in the fuel consumption and/or mission payload. The percentage change and the chosen parameters are given in Table 1.

The aerodynamic mismatch is introduced to recreate the uncertainty that exists for aerodynamic database (intrinsically very difficult to identify) and to avoid perfect cancellation of the dynamics due to their inversion. Typically, fixed percentage changes are applied to the moments and forces but sometimes, and more accurately, Mach or altitude based percentage profiles are applied to some of the stability derivatives and/or to the lift and drag coefficients. In the present case, we follow the uncertainty characterization offered in (Cobleigh, R.B., 1998) but adapted to our purposes. Figure 3 shows two of the aerodynamic coefficients' uncertainty profiles used to perturb the Hopper aerodynamic database during the Monte-Carlo campaign.

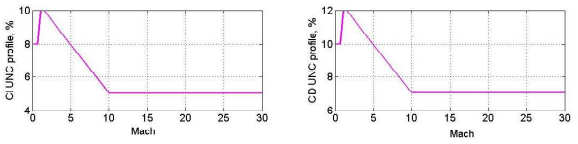

Fig. 3. Aerodynamic coefficients percentage uncertainty profiles.

For each shot, all the aerodynamic coefficient's uncertainty profiles are scaled by different random variables (uniformly distributed between $\pm$ 1 and each with a different seed). Furthermore, in order to physically motivate the uncertainty, the lift and drag uncertainties thus obtained are compared, and re-calculated if needed, to a Lift-to-Drag ratio uncertainty profile similarly obtained. This will ensure that no unrealistic lift and drag coefficient uncertainty is obtained (see (Cobleigh, R.B., 1998) for more details).

It is important to highlight, that each simulation run is completely automated (i.e. no phase patching is performed after simulation nor operator intervention once the simulations are started). This is an important consideration which showcases the effectiveness of the controller for complete automated control of the re-entry trajectory.

Figures 4 $\rightarrow$ 7 show the results from the Monte Carlo campaign using 130 shots (each run takes about 30 minutes on a Pentium 4 3.0GHz with 1.024Mb RAM).

Figure 5 (in next page) shows the main rotational and translational responses. As it is easily observed, the results are very satisfactory achieving level 1 or level 2 tracking performance objectives (observe the errors associated to the aerodynamic angles).

Figures 4 and 6 show the corresponding RCS and aerosurfaces deflections together with their magnitude saturation bounds. Note that the z-axis RCS saturate slightly (but achieving a performance level 2) around the 750-800 sec time range. This range corresponds to the high-speed bank reversal (of a magnitude close to 85 degrees) which is quite a strong manoeuvre. Similarly, saturation of the flap, left-inboard (ELI) and right-inboard (ERI) surfaces are observed for the first part of the re-entry trajectory. This is acceptable since these surfaces are used for trimming mainly, and the established optimal trim strategy is to saturate first flap and if needed then the other inboard surfaces.

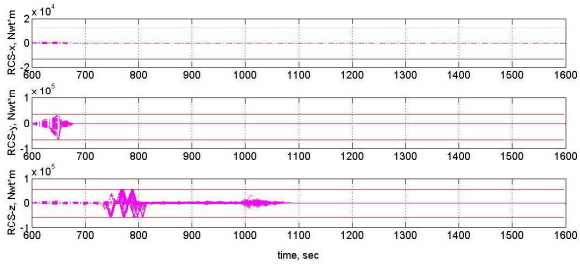

Fig. 4. Monte Carlo (130 sims): RCS demands.

For completeness, Figure 7 shows the random population for the parametric uncertainty versus the shot number –together with the maximum percentage uncertainty bounds (the same from Table 1)– for two of the uncertain parameters.

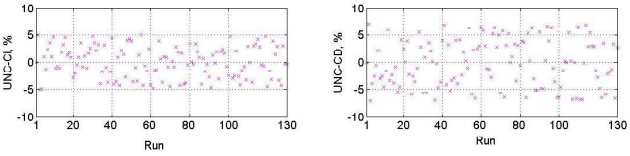

Fig. 7. Monte Carlo (130 sims): parametric uncertainty population.

6. CONCLUSIONS

In this paper the NDI design of a fully automated re-entry attitude control for the Hopper RLV concept has been presented. The NDI design is characterized by *i*) a four step-approach with a mixed Wind/Body-axes formulation (that facilitates the PID design by decoupling the axis motions); *ii*) a moment allocation scheme that automates the transitions for the different flight phases, and *iii*) a NDI inversion step that uses the redundancy on actuation to perform two inversions (one for the trim surfaces and the other for the flight surfaces).

The approach presented yields a controller that has been validated using a realistic, high-fidelity DKE simulator for the Hopper RLV. The time responses (subject to parametric & aerodynamic uncertainty, noise corruption, actuator limits and atmospheric environment) show that the design successfully tracks the optimal reference trajectory satisfying all control objectives for the duration of the re-entry flight.

7. ACKNOWLEDGMENT

The authors would like to acknowledge the fruitful discussions and help of Eric Bornschlegl, ESA tech-

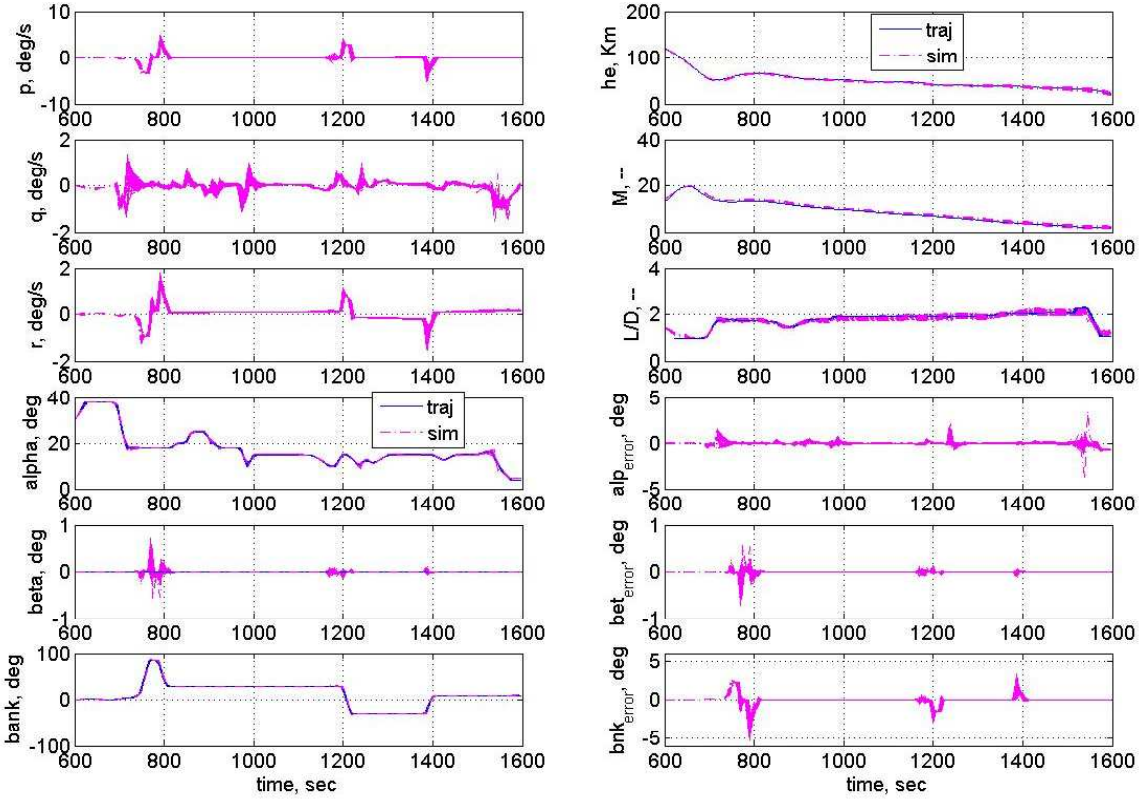

Fig. 5. Monte Carlo (130 sims): main rotational and translational time responses.

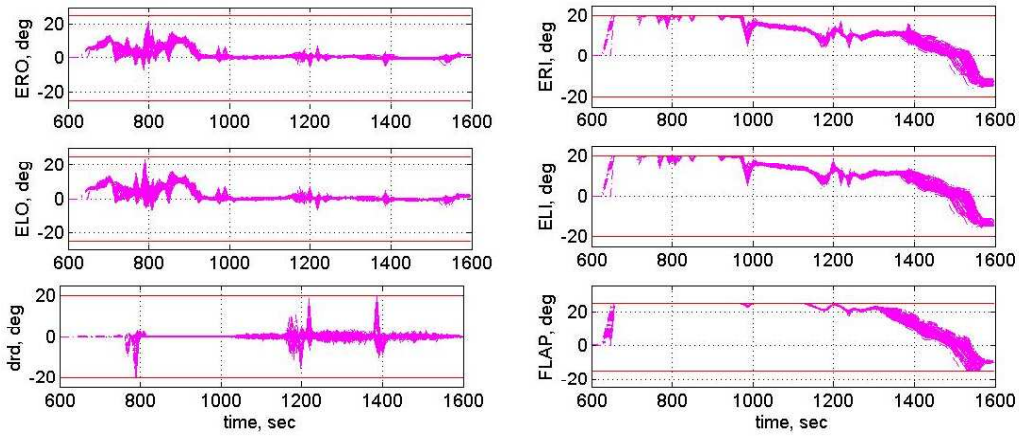

Fig. 6. Monte Carlo (130 sims): aerodynamic and Hopper surfaces deflections.

nical contract monitor of the project, and of Samir Bennani from ESA/ESTEC.

REFERENCES

Cobleigh, R.B. (1998). Development of the X-33 Aerodynamic Uncertainty Model. Technical Report NASA TP-206544. NASA Dryden Flight Research Center.

Da Costa, R.R., Chu, Q.P. and Mulder, J.A. (2003). Re-entry Flight Controller Design Using Nonlinear Dynamic Inversion. *Journal of Spacecraft and Rockets*.

Durham, W.C. (2001). *Aircraft Dynamics and Control*. Virginia Polytechnic Institute.

Honeywell and Lockheed Martin (1996). Application of Multivariable Control Theory to Aircraft Control Laws. Technical Report WL-TR-96-3099. Flight Dynamics Directorate, Wright Laboratory. Wright-Patterson Air Force Base, OH.

Ito, D., Georgie, J., Valasek, J. and Ward, D.ST (2002). Re-entry Vehicle Flight Controls Design Guidelines: Dynamic Inversion. Technical Report NASA/TP-2002-210771. Flight Simulation Laboratory, Texas A&M University.

Vu, B.D. (1997). Nonlinear Dynamic Inversion Control. In: *Robust Flight Control: A Design Challenge* (Magni, J.F., Bennani, S. and Terlouw, J., Eds.). Chap. 9. Springer-Verlag. Lecture Notes in Control and Information Sciences.

Zhou, K., Doyle, J.C. and Glover, K. (1996). *Robust and Optimal Control*. Prenticel-Hall. Englewood Cliffs, NJ.